

## THE ROLE OF GALAXY INTERACTION IN ENVIRONMENTAL DEPENDENCE OF THE STAR FORMATION ACTIVITY AT $Z \simeq 1.2$

Y. IDEUE<sup>1</sup>, Y. TANIGUCHI<sup>2</sup>, T. NAGAO<sup>3,4</sup>, Y. SHIOYA<sup>2</sup>, M. KAJISAWA<sup>2</sup>, J. R. TRUMP<sup>5</sup>, D. VERGANI<sup>6</sup>, A. IOVINO<sup>7</sup>, A. M. KOEKEMOER<sup>8</sup>, O. LE FÈVRE<sup>9</sup>, O. ILBERT<sup>10</sup>, AND N. Z. SCOVILLE<sup>11</sup>

*Draft version October 14, 2018*

### ABSTRACT

In order to understand environmental effects on star formation in high-redshift galaxies, we investigate the physical relationships between the star formation activity, stellar mass, and environment for  $z \simeq 1.2$  galaxies in the 2 deg<sup>2</sup> COSMOS field\*. We estimate star formation using the [O II] $\lambda$ 3727 emission line and environment from the local galaxy density. Our analysis shows that for massive galaxies ( $M_* \gtrsim 10^{10} M_\odot$ ), the fraction of [O II] emitters in high-density environments ( $\Sigma_{10\text{th}} \gtrsim 3.9 \text{ Mpc}^{-2}$ ) is  $1.7 \pm 0.4$  times higher than in low-density environments ( $\Sigma_{10\text{th}} \lesssim 1.5 \text{ Mpc}^{-2}$ ), while the [O II] emitter fraction does not depend on environment for low-mass  $M_* \lesssim 10^{10} M_\odot$  galaxies. In order to understand what drives these trends, we investigate the role of companion galaxies in our sample. We find that the fraction of [O II] emitters in galaxies with companions is  $2.4 \pm 0.5$  times as high as that in galaxies without companions at  $M_* \gtrsim 10^{10} M_\odot$ . In addition, massive galaxies are more likely to have companions in high-density environments. However, although the *number* of star forming galaxies increases for massive galaxies with close companions and in dense environments, the *average* star formation rate of star forming galaxies at a given mass is independent of environment and the presence/absence of a close companion. These results suggest that interactions and/or mergers in high-density environment could induce star formation in massive galaxies at  $z \sim 1.2$ , increasing the fraction of star-forming galaxies with  $M_* \gtrsim 10^{10} M_\odot$ .

*Subject headings:* galaxies: evolution – galaxies: formation – galaxies: high-redshift – galaxies: interactions

### 1. INTRODUCTION

A key question in understanding the formation and evolution of galaxies is to find what physical parameters are most sensitive to the star formation process in galaxies; e.g., how the star formation activity depends on the environment, and how the relation between star formation and environment changes during the course of galaxy evolution over 10 Gyrs. Observational properties of galaxies in the local universe have been extensively studied in the past. Typically, actively star-forming galaxies in the local universe have lower masses than passive galaxies and the most massive galaxies tend to be inactive for star formation (so-called mass-downsizing; Cowie et al. 1996). In addition, the star formation activity strongly depends on environment: star formation rate (SFR) decreases with increasing galaxy density (e.g., Lewis et al. 2002; Gomez et al. 2003; Kauffmann et al. 2004; Mahajan et al. 2010) and the fraction of star-forming galaxies also decreases with increasing galaxy density (e.g., Carter et al. 2001; Balogh et al. 2004; Mateus & Sodr e 2004). The fraction of early-type (passive) galaxies is higher in higher-density regions while the fraction of late-type (star-forming) ones is lower in such environment, called the “morphology-density relation” and consistent with the above results (e.g., Dressler 1980; Dressler et al. 1997; Goto et al. 2003; Capak et al. 2007). These findings indicate that the star formation activity in galaxies is strongly related to both the stellar mass and their environment.

cedex 13, France

<sup>11</sup> Department of Astronomy, MS 105-24, California Institute of Technology, Pasadena, CA 91125

\* Based on observations with the NASA/ESA *Hubble Space Telescope*, obtained at the Space Telescope Science Institute, which is operated by AURA Inc, under NASA contract NAS 5-26555. Also based on observations made with the Spitzer Space Telescope, which is operated by the Jet Propulsion Laboratory, California Institute of Technology, under NASA contract 1407. Also based on data collected at; the Subaru Telescope, which is operated by the National Astronomical Observatory of Japan; the XMM-Newton, an ESA science mission with instruments and contributions directly funded by ESA Member States and NASA; the European Southern Observatory under Large Program 175.A-0839, Chile; Kitt Peak National Observatory, Cerro Tololo Inter-American Observatory and the National Optical Astronomy Observatory, which are operated by the Association of Universities for Research in Astronomy, Inc. (AURA) under cooperative agreement with the National Science Foundation; and the Canada-France-Hawaii Telescope with MegaPrime/MegaCam operated as a joint project by the CFHT Corporation, CEA/DAPNIA, the NRC and CADC of Canada, the CNRS of France, TERAPIX and the Univ. of Hawaii.

<sup>1</sup> Graduate School of Science and Engineering, Ehime University, Bunkyo-cho, Matsuyama 790-8577, Japan: *e-mail: ideue@cosmos.phys.sci.ehime-u.ac.jp*

<sup>2</sup> Research Center for Space and Cosmic Evolution, Ehime University, Bunkyo-cho, Matsuyama 790-8577, Japan

<sup>3</sup> The Hakubi Project, Kyoto University, Yoshida-Ushinomiya-cho, Sakyo-ku, Kyoto 606-8302, Japan

<sup>4</sup> Department of Astronomy, Kyoto University, Kitashirakawa-Oiwake-cho, Sakyo-ku, Kyoto 606-8502, Japan

<sup>5</sup> UCO/Lick, UC Santa Cruz, Santa Cruz, CA 95064 USA

<sup>6</sup> INAF-Osservatorio Astronomico di Bologna, Via Ranzani 1, I-40127, Bologna, Italy

<sup>7</sup> INAF-Osservatorio Astronomico di Brera, Via Brera 28, I-20159 Milano, Italy

<sup>8</sup> Space Telescope Science Institute, 3700 San Martin Drive, Baltimore, MD 21218

<sup>9</sup> Laboratoire d’Astrophysique de Marseille, CNRS-Universit e d’Aix-Marseille, 38 rue Frederic Joliot Curie, F-13388 Marseille, France

<sup>10</sup> Observatoire de Marseille-Provence, Pole de l’Etoile Site de Chiateau-Gombert, 38 rue Frederic Joliot-Curie, 13388 Marseille

On the other hand, it is well known that the star formation rate density (SFRD) steeply increases in the first  $\sim 2$  Gyrs, peaks at  $z \sim 1-3$ , and then decreases by an order of magnitude toward the present day (e.g., Madau et al. 1996; Lilly et al. 1996; Shioya et al. 2008; Bouwens et al. 2009). These results suggest that the redshift range of  $z \sim 1-3$  is the key epoch for the most active cosmic star formation in the history of universe. Therefore, studies of galaxies at  $1 < z < 3$  are important for understanding galaxy evolution. In recent years, wide and deep surveys have allowed us to study star formation activity in  $z \gtrsim 1$  galaxies. For example, Elbaz et al. (2007) and Cooper et al. (2008) studied the relation between the star formation rate (SFR) in galaxies and the environment at  $z \sim 1$ , in the Great Observatories Origins Deep Survey (GOODS; Giavalisco et al. 2004) and the DEEP2 Galaxy Redshift Survey (DEEP2; Davis et al. 2003). These studies showed that the average star formation rate increases with increasing galaxy density (Elbaz et al. 2007; Cooper et al. 2008). We also investigated the relation between the fraction of star-forming galaxies with [O II]  $\lambda 3727$  emission (hereafter “[O II] emitters”) and the local galaxy density at  $z \simeq 1.2$  in the Cosmic Evolution Survey (COSMOS; Scoville et al. 2007a; Koekemoer et al. 2007) and found that the fraction of star-forming galaxies in high-density regions is as high as that in low-density regions (Ideue et al. 2009; hereafter “Paper I”). Similar trends were also reported by other observational studies in groups of galaxies (Iovino et al. 2010; Li et al. 2011; Sobral et al. 2011) and cluster environments (Hayashi et al. 2010; Hilton et al. 2010) at  $z \gtrsim 1$ . Since the fraction of star-forming galaxies decreases with increasing galaxy density in the local universe as mentioned above, these results suggest that the relationship between the star formation activity in galaxies and their environment dramatically changed from  $z \sim 1$  to the present day. On the other hand, many studies suggest that the star formation activity or the fraction of star-forming galaxies also strongly depends on stellar mass even at  $z \gtrsim 1$  (e.g., Noeske et al. 2007; Elbaz et al. 2007; Ilbert et al. 2010). Therefore, it is important to investigate the relationships between the star formation activity, the stellar mass of galaxies, and the environment at  $z \sim 1$ , in order to reveal the origin of the observed difference in the environmental dependence of the star formation activity between  $z \sim 0$  and  $z \sim 1$ .

In this paper, we focus on the relationships between the star formation, stellar mass, and environment of galaxies at  $z \simeq 1.2$  in the COSMOS field. We have already carried out Subaru imaging observations of the COSMOS field (Taniguchi et al. 2007). We can obtain the sample of [O II] emitters in the COSMOS field by using a narrowband filter NB816 ( $\lambda_c = 8150 \text{ \AA}$  and  $\Delta\lambda(\text{FWHM}) = 120 \text{ \AA}$ , see Takahashi et al. 2007) and estimate their SFR by using the [O II] luminosity. The [O II] emission line provides a good estimator of the star formation in galaxies at intermediate redshift (e.g., Kennicutt 1998; Jansen et al. 2001). The stellar mass in galaxies in the COSMOS field was obtained from the fitting of their spectral energy distributions (SEDs; Ilbert et al. 2010). Thanks to the very large survey area ( $\sim 2 \text{ deg}^2$ ) of the COSMOS field, we are able to obtain an unbiased picture of the star formation activity in galaxies, avoiding the cosmic vari-

ance effect. Indeed, the COSMOS field includes various regions with a wide range of galaxy density (e.g., Scoville et al. 2007a, 2007b; Takahashi et al. 2007), which enables us to investigate systematically the environmental effects on galaxy properties.

This paper is organized as follows. In section 2, we describe the sample selection and possible contamination of the [O II] emitter sample. Descriptions of the measurements of local galaxy density, stellar mass, and SFR are presented in section 3. We investigate the dependence of star formation on environment and stellar mass, and the effect of close companions on the star formation activity, for our sample at  $z \simeq 1.2$  in section 4. In section 5, we summarize our findings and discuss implications of our results on the evolution of galaxies from  $z \sim 1.2$  to  $z \sim 0$ . Throughout this paper, magnitudes are given in the AB system. We adopt a flat universe with the following cosmological parameters;  $\Omega_{\text{matter}} = 0.3$ ,  $\Omega_{\Lambda} = 0.7$ , and  $H_0 = 70 \text{ km s}^{-1} \text{ Mpc}^{-1}$ .

## 2. THE SAMPLE

### 2.1. Catalog

The COSMOS field has multi-wavelength photometric data over an area of  $\sim 2 \text{ deg}^2$  from X-ray to radio. We use the COSMOS intermediate- and broad-band photometry catalog which includes 16 broad, 12 intermediate, and 2 narrow bands (Capak et al. 2011, in preparation: hereafter “the COSMOS photometric catalog”). We also use the photometric redshift catalog (Ilbert et al. 2009: hereafter “the COSMOS photo- $z$  catalog”) which includes 937013 objects whose total  $i$  magnitudes (Subaru  $i'$  or CFHT  $i^*$ ) are brighter than 26 mag. Photometric redshifts in COSMOS are computed using the 25 optical bands, plus 2 GALEX and 4 Spitzer/IRAC bands (Ilbert et al. 2009, see also Section 3.2).

### 2.2. Sample Selection

In order to select [O II] emitters at  $z \sim 1.2$ , we use the photometric data of  $i'$ ,  $z'$ , and NB816 bands taken on the Subaru Telescope and those of  $i^*$ -band taken on the Canada France Hawaii Telescope in the COSMOS photometric catalog (Capak et al. 2011, in preparation). We also use the photometric redshifts from the COSMOS photo- $z$  catalog (Ilbert et al. 2009).

Using the NB816-band photometric data, Takahashi et al. (2007) extracted a sample of [O II] emitters at  $1.17 < z < 1.20$ . Here we additionally extract a sample of non-[O II]-detected galaxies in the same  $1.17 < z_{\text{ph}} < 1.20$  redshift range. Since fainter galaxies have larger photo- $z$  errors, we select only galaxies with  $i' < 24$ , for which the photo- $z$  error is  $\sigma_{\Delta z} = 0.026$  at  $z \sim 1.2$ . Consequently, we obtain 1654  $i$ -selected galaxies with  $1.17 < z_{\text{ph}} < 1.20$ .

Among the 1654 galaxies, we select galaxies satisfying the following criteria as [O II] emitters:

$$iz - NB816 > \max(0.2, 3\sigma_{iz-NB816}), \quad (1)$$

where

$$3\sigma_{iz-NB816} = -2.5 \log(1 - \sqrt{f_{3\sigma_{NB816}}^2 + f_{3\sigma_{iz}}^2 / f_{NB816}}), \quad (2)$$

and

$$f_{iz} = 0.57f_i + 0.43f_z. \quad (3)$$

Note that  $iz - NB816 = 0.2$  corresponds to  $EW([\text{O II}]) \approx 12 \text{ \AA}$  in the rest frame, where  $iz$  is the matched continuum for the central wavelength of NB816 filter (see Takahashi et al. 2007).

We obtain 932 [O II] emitters among the photo- $z$  selected galaxies with  $i' < 24$ . The remaining 722 objects are galaxies without a significant narrow-band excess by the [O II] emission line; their rest-frame [O II] emission equivalent width is  $EW([\text{O II}]) < 12 \text{ \AA}$  and we designate them “non-[O II] emitters” in this paper.

### 2.3. Contamination and Incompleteness due to Photometric Redshift Errors

As mentioned in the previous section, we selected our photo- $z$  sample and [O II] emitters at  $z \simeq 1.2$  using the photometric redshift and eq (1). Although the contamination is thought to be small due to the fairly accurate photo- $z$  (Ilbert et al. 2009), we examine how our photo- $z$  samples are contaminated by foreground or background objects, using spectroscopic redshifts (spec- $z$ ) from the zCOSMOS redshift catalog (Lilly et al. 2007; Lilly et al. in prep). The spec- $z$  is available for 48 [O II] emitters and 37 non-[O II] emitters in our photo- $z$  sample. Among these objects, 44 [O II] emitters and 24 non-[O II] emitters have spec- $z$  within our target redshift range,  $z = 1.17 - 1.20$ , while the remaining objects have  $z_{\text{sp}} < 1.17$  or  $z_{\text{sp}} > 1.20$ . This means that the contamination rates for the [O II] emitter and non-[O II] emitter samples are 8% (4/48) and 35% (13/37), respectively. Thus, the contamination rate for our photo- $z$  sample (932 [O II] emitters + 722 non-[O II] emitters) is expected to be  $\sim 20\%$ .

We also estimate the incompleteness of our photo- $z$  sample, using 90 objects with  $i' < 24$  and  $z_{\text{sp}} = 1.17 - 1.20$ . Only 69 objects among them have  $z_{\text{ph}} = 1.17 - 1.20$ , and so the incompleteness is 23% (21/90). In order to investigate how incomplete our [O II] emitter and non-[O II] emitter samples are, we divided the 90 objects with  $i' < 24$  and  $z_{\text{sp}} = 1.17 - 1.20$  into the narrow-band excess objects and the others, using eq. (1). As a result, 47 objects are narrow-band excess objects, and the other 43 objects do not show a significant narrow-band excess. All of the 47 narrow-band excess objects with  $z_{\text{sp}} = 1.17 - 1.20$  have  $z_{\text{ph}} = 1.17 - 1.20$  and are selected as [O II] emitters, suggesting that photometric redshifts are nearly complete for the [O II] emitters. On the other hand, 22 out of 43 objects without a significant narrow-band excess have  $z_{\text{ph}} = 1.17 - 1.20$ . Thus the incompleteness rates for the [O II] emitter and non-[O II] emitter samples are estimated to be 0% (0/47) and 49% (21/43), respectively.

In summary, the contamination and incompleteness rates for our photo- $z$  sample are  $\sim 20\%$ . To keep the uniformity of photo- $z$  selected sample, we neither exclude the contamination nor add the missed objects into our sample, using the spectroscopic information. We will discuss how the contamination and incompleteness due to the photometric redshift errors for our photo- $z$  and [O II] emitter samples affect our results in Section 4.

### 2.4. AGN Contamination in [O II] Emitter Sample

Since active galactic nuclei (AGNs) also show emission lines including [O II] in general, we have to consider

the contribution of such AGNs in our analysis. Here we try to estimate possible AGN contamination in our [O II] emitter sample by taking account of the difference of SEDs between AGNs and star-forming galaxies.

Stern et al. (2005) found that AGNs can be distinguished from star-forming galaxies using a [3.6] – [4.5] vs. [5.8] – [8.0] color-color diagram. While the ultraviolet to mid-infrared ( $\lambda < 5 \mu\text{m}$ ) continuum of star-forming galaxies is the composite stellar black body, an AGN continuum is well fit by a power law. Accordingly the infrared SED of AGNs tends to be systematically redder than star-forming galaxies. Although Stern et al. (2005) defined the AGN selection criteria for objects at  $z = 0 - 4$ , some star-forming galaxies at  $z \sim 1.2$  could be misidentified as AGNs by their criteria. In order to avoid this situation, we have newly defined our own AGN criteria for objects at  $z \simeq 1.2$  examining Figures 2 and 3 in Stern et al. (2005). Our criteria are  $([3.6] - [4.5])_{\text{AB}} > 0$  and  $([5.8] - [8.0])_{\text{AB}} > 0$ , which are derived from the four IRAC bands (3.6, 4.5, 5.8, and 8.0  $\mu\text{m}$ ) in the COSMOS photometric catalog.

We apply these criteria for the 587 [O II] emitters detected in all the IRAC bands, and then find that 21 objects are identified as AGN candidates. Of the 345 objects without detection in all four IRAC bands, 244 are detected in both 3.6 and 4.5  $\mu\text{m}$ . For these we are able to examine AGN candidates only by using the  $([3.6] - [4.5])_{\text{AB}}$  color and  $[3.6]_{\text{AB}} - [4.5]_{\text{AB}} > 0$ ; see Figure 1 in Stern et al. (2005). We find that 18 of the 244 galaxies are identified as AGNs by this criterion. Thus, the total number of the AGN candidates in our [O II] emitter sample is 39, giving the possible AGN contamination rate of 4.7%.

It is noted, however, that our mid-infrared color criteria described above may not be useful in identification of LINERs that are also popular [O II] emitters in the local universe. For such cases, we are able to use optical colors to estimate the contamination from LINERs since host galaxies of LINERs tend to show red optical colors. For example, Yan et al. (2006) found that most [O II] emitters with red optical colors tend to have the LINER activity rather than star formation. Lemaux et al. (2010) also found that most of [O II] emitters on the so-called red sequence at  $z = 0.8 - 0.9$  are identified as either LINERs or Seyferts. In order to examine the contamination from LINERs in our [O II] emitter sample, we investigate the SED of the [O II] emitters and found that almost all galaxies show blue colors, being comparable to those of starburst or local Sd – Sdm-type galaxies. Therefore, we conclude that the contamination from LINERs is negligibly small in our sample.

Thus the possible fraction of AGN in our [O II] emitters is  $\sim 5\%$ . This is roughly consistent with the result of Garn et al. (2010) who studied the star formation activity in galaxies at  $z = 0.84$  using a sample of H $\alpha$  emitters and found that the AGN fraction is 5-11%.

Because the AGN contamination is negligibly small, we do not exclude the AGN candidates from the [O II] emitter sample in the following analysis. However we additionally performed the same analysis given in Section 4 for the sample without the AGN candidates and found the same results, confirming that the contamination from AGNs is negligibly small.

### 3. MEASUREMENT OF LOCAL DENSITY, STELLAR MASS, SFR

#### 3.1. Local Galaxy Density

In order to investigate the relation between the star formation activity in galaxies and their environment, we quantify the environment from the observational data. We adopt the projected  $N$ th-nearest-neighbor surface density since this density has been often used as an indicator of the galaxy environment in a number of previous investigators (e.g., Dressler 1980; Postman et al. 2005). It is also noted that such projected density measurements based on photo- $z$  are useful in detecting the so-called large-scale structures and reconstructing the overdensity (Scoville et al. 2007b).

To be consistent with previous studies (e.g., Dressler 1980; Capak et al. 2007; Feruglio et al. 2010), we use the 10th nearest neighbor in our analysis. The local galaxy density is calculated by using the projected proper distance to the 10th nearest neighbor ( $r_{10\text{th}}$  in Mpc) as

$$\Sigma_{10\text{th}} = \frac{11}{\pi r_{10\text{th}}^2}. \quad (4)$$

We compute the projected densities for our sample galaxies using the COSMOS photo- $z$  catalog. We use a redshift slice centered on each sample galaxy with a width of  $\pm\sigma_{\Delta z}$  ( $\sigma_{\Delta z} = 0.026$  for  $z \sim 1.2$ ; Ilbert et al. 2009). Note that we use only galaxies with  $i' < 24$  in a given redshift slice to secure the photo- $z$  accuracy in the estimate of the projected densities. For 204 galaxies near the edge of our survey field, the  $r_{10\text{th}}$  is greater than the distance from the object to the field edge. We do not use them in the later analysis, since we cannot estimate their local galaxy densities accurately.

In Figure 1, we show the distribution of the local galaxy density for our photo- $z$  selected sample. The local galaxy density for our sample galaxies ranges over  $-0.3 \lesssim \log \Sigma_{10\text{th}} \lesssim 1.1$ . In order to investigate environmental effects on star formation in section 4, we define three environment bins: low-density ( $\log \Sigma_{10\text{th}} \leq 0.185$ ), intermediate ( $0.185 < \log \Sigma_{10\text{th}} < 0.585$ ), and high-density ( $0.585 \leq \log \Sigma_{10\text{th}}$ ). The number of galaxies in each environment bin is 464, 820, and 162 for the low-, intermediate-, and high-density environment, respectively. We note that the intermediate-density environment includes the mean local galaxy density in our sample ( $\langle \log \Sigma_{10\text{th}} \rangle = 0.3$ ).

#### 3.2. Stellar Mass and Star Formation Rate

In this study, we use stellar mass estimates which come from SED fitting by Ilbert et al. (2010). The COSMOS 31 photometric-band data (including the IRAC mid-infrared data) are fit with stellar population synthesis models (Bruzual and Charlot 2003), assuming a Chabrier (2003) IMF and exponentially declining star formation histories (see Ilbert et al. 2010 for details).

To estimate the SFR, we use the [O II] $\lambda 3727$  emission-line luminosity. We measure the [O II] luminosity from the line flux which is estimated by using the flux densities in  $i'$ ,  $z'$ , and NB816 as adopted in Takahashi et al. (2007), given by

$$f_{\text{line}} = \Delta \text{NB816} \frac{f_{\text{NB816}} - f_{iz}}{1 - 0.57(\Delta \text{NB816}/\Delta i)}, \quad (5)$$

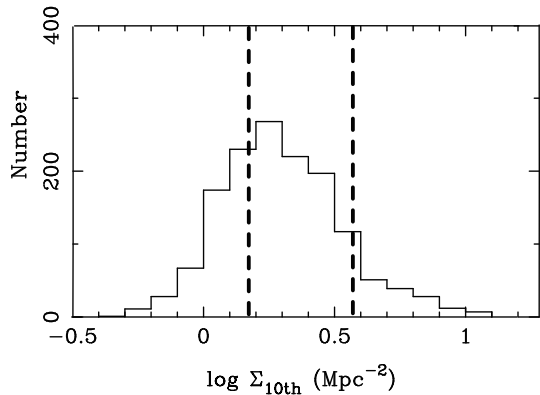


FIG. 1.— The histograms show the numbers of galaxies with  $i' < 24$  and  $z_{\text{ph}} = 1.17 - 1.20$  in the COSMOS field as a function of the local galaxy density derived from the distance to the 10th nearest neighbor. The vertical dashed lines show the boundaries between three environments.

where  $\Delta \text{NB816}$  and  $\Delta i$  are the effective bandwidth of the NB816 and  $i'$  filters, respectively. The [O II] luminosity is estimated from the line flux by  $L([\text{O II}]) = 4\pi d_L^2 f_{\text{cor}}([\text{O II}])$ . In this procedure, we assume that all the [O II] $\lambda 3727$  emitters are located at  $z = 1.187$ , the redshift corresponding to the central wavelength of NB816 filter, setting the luminosity distance as  $d_L = 8190$  Mpc.

We then apply an extinction correction to the [O II] luminosity of each object. Previous studies have generally assumed  $A_{\text{H}\alpha} = 1.0$ , which is estimated from observations of local star-forming galaxies (Kennicutt 1983; Kennicutt 1998; Hopkins 2004). However, Gilbank et al (2010; hereafter G10) found that there is a stellar-mass dependence of the dust extinction of nebula emission lines, with  $A_{\text{H}\alpha} = 1.0$  overestimating the line luminosity for low-mass galaxies and underestimating it for high-mass galaxies. This effect should be taken into account in the estimate of SFR, since we investigate the dependence of SFR on stellar mass in this study. We calculate  $A_{\text{H}\alpha}$  for each [O II] emitter using the relation between  $A_{\text{H}\alpha}$  and stellar mass obtained by G10:

$$A_{\text{H}\alpha} = -51.201 - 11.199 \log M_* + 0.615 (\log M_*)^2 (M_* > 10^9 M_\odot) \quad (6)$$

$$A_{\text{H}\alpha} = 0.225 (M_* < 10^9 M_\odot). \quad (7)$$

Note, however, that we adopt

$$A_{\text{H}\alpha} = 1.101 \log M_* - 10.299 (M_* > 10^{10} M_\odot). \quad (8)$$

because  $A_{\text{H}\alpha}$  estimated from eq. (9) in G10 seems to overestimate at  $M_* > 10^{10} M_\odot$  (see Figure 4 in G10). We derive  $A_{[\text{O II}]}$  from  $A_{\text{H}\alpha}$  using the Galactic extinction curve (Cardelli et al. 1989). The extinction-corrected [O II] luminosity is given by

$$L_{\text{cor}}([\text{O II}]) = L_{\text{line}} \times 10^{0.4A_{[\text{O II}]}}. \quad (9)$$

We estimate the SFR from the [O II] luminosity using the Kennicutt (1998) relation:

$$\text{SFR} (M_\odot \text{ yr}^{-1}) = 1.41 \times 10^{-41} L([\text{O II}]) (\text{ergs s}^{-1}). \quad (10)$$

In the following analysis, we use 1446 galaxies (824 [O II] emitters and 622 non-[O II] emitters) with  $M_* > 10^8 M_\odot$  for which the local galaxy density is available. A summary of all galaxy samples used in our analysis is given in Table 1.

TABLE 1  
THE NUMBER OF GALAXIES IN EACH ENVIRONMENTS AND MASS BINS

$\log M_*(M_\odot)$	All samples			[O II] emitters			non-[O II] emitters		
	Low	Intermediate	High	Low	Intermediate	High	Low	Intermediate	High
8 – 8.5	0	4	0	0	3	0	0	1	0
8.5 – 9	19	30	9	13	20	8	6	10	1
9 – 9.5	103	172	24	97	155	23	6	17	1
9.5 – 10	147	281	50	110	228	39	37	53	11
10 – 10.5	82	139	48	33	55	23	49	84	25
10.5 – 11	80	141	24	5	5	4	75	136	20
11 – 11.5	32	51	7	1	2	0	31	49	7
11.5 – 12	1	2	0	0	0	0	1	2	0
Total	464	820	162	259	468	97	205	352	65

#### 4. RESULTS

##### 4.1. The relations between star formation, stellar mass, and environment

In this section, we study the relations between star formation, stellar mass, and environment. In Figure 2, we show the fraction of the [O II] emitters in the photo- $z$  selected sample (hereafter, “[O II] fraction”) as a function of stellar mass for the three different environments. In all environments, the [O II] fraction decreases with increasing stellar mass, indicating that most low-mass galaxies are star-forming while non-star-forming galaxies dominate at high mass. This suggests that mass-downsizing is already in place at  $z \simeq 1.2$ . Several studies have reported similar results for galaxies at  $z \sim 0.8$  (Iovino et al. 2010; Sobral et al. 2011).

Next we focus on the environmental dependence of the [O II] fraction. While there is no environmental dependence of the [O II] fraction in low-mass bins ( $M_* \lesssim 10^{10} M_\odot$ ), the [O II] fraction in the high-density environment is a little higher than that in the intermediate- and low-density environments in high-mass bins ( $M_* \sim 10^{10} - 10^{11} M_\odot$ ), although the uncertainty for the high-density environment is relatively large due to the small number statistics. We estimate the [O II] fraction in the high- and low-density environment for massive galaxies ( $M_* \gtrsim 10^{10} M_\odot$ ). We then find the [O II] fraction in the high-density environment is  $1.7 \pm 0.4$  times higher than that in the low-density environment. This may indicate that the star formation activity in relatively massive galaxies is enhanced in high-density regions.

Figure 3 shows the distribution of stellar mass for the [O II] emitters in the three different environments. The distribution for [O II] emitters in the high-density environment appears to be slightly skewed toward high mass, compared with those for the lower-density environments. We estimate the fraction of high-mass galaxies ( $M_* > 10^{10} M_\odot$ ) in the [O II] emitter sample for the low-, intermediate-, and high-density environments are 15%, 13%, and 28%, respectively. Indeed, the fraction of high-mass [O II] emitters in the high-density environment is more than twice as high as the low-, and intermediate-density environments. We apply the Kolmogorov-Smirnov (K-S) test to the distribution of stellar mass for the low- and high-density environments. The K-S test gives a 1.5% probability of the two distributions being drawn from the same parent distribution. This seems to be consistent with the above result: the fraction of [O II] emitters with  $M_* > 10^{10} M_\odot$  is high-

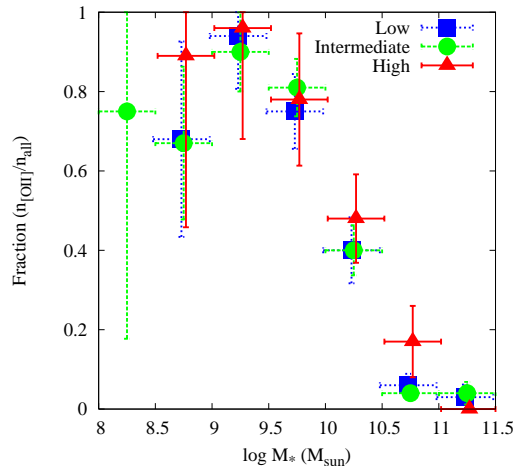


FIG. 2.— The fraction of [O II] emitters in the photo- $z$  selected sample as a function of stellar mass in the three different environments. The blue squares, green circles, and red triangles represent the low-, intermediate-, and high-density environments, respectively. The error bars along the vertical axis are  $1 \sigma$  Poisson errors, and those along the x-axis indicate the bin widths. Data points for the different environments are plotted with small horizontal offsets for clarity.

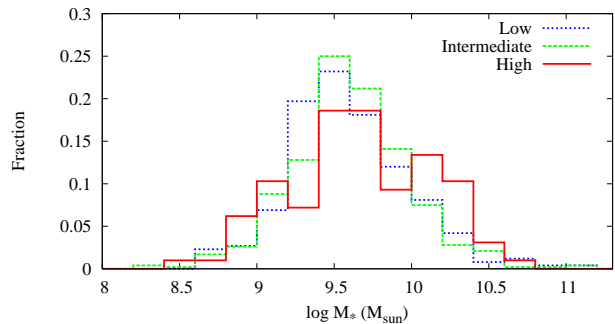


FIG. 3.— The normalized histograms of stellar mass for the [O II] emitter sample. The blue dotted, green dashed, blue solid lines represent the low-, intermediate-, high-density environments, respectively.

est in the high-density environment because the shape of the stellar mass function for all of our photo- $z$  selected galaxies is similar among the different environments over  $M_* \gtrsim 10^9 M_\odot$ .

We investigate the average SFR as a function of stellar mass for [O II] emitters in the three environments

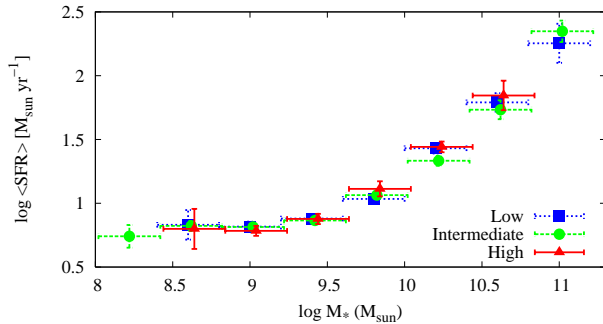


FIG. 4.— The average SFR of [O II] emitters as a function of stellar mass in the three different environment. Symbols are the same as Figure 2. The error bars along the y-axis are  $1\sigma$  errors based on the standard deviation, and those along the x-axis indicate the size of bins. Data points for the different environments are plotted with small horizontal offsets for clarity.

(Figure 4). The linear fit gives the following relations:  $\log \langle \text{SFR} \rangle = (0.60 \pm 0.11) \times \log M_* - (4.71 \pm 1.09)$  for the low-density environment,  $(0.54 \pm 0.12) \times \log M_* - (4.20 \pm 1.18)$  for the intermediate-density environment, and  $(0.59 \pm 0.08) \times \log M_* - (4.56 \pm 0.78)$  for the high-density environment. These results show the average SFR strongly correlates with the stellar mass, consistent with the results in previous studies (e.g., Elbaz et al. 2007; Daddi et al. 2007). We also find that the relation between SFR and stellar mass in our star-forming galaxies does not depend on environment. These results imply that there is no environmental effect on the *strength* of star formation activity in star-forming galaxies, although environment does affect the *fraction* of star-forming galaxies among the total population (perhaps switching and quenching star formation).

#### 4.2. Role of interactions and/or mergers

In Paper I, we found that the fraction of galaxies with a close companion increases with increasing local galaxy density. Since galaxy interactions and mergers can trigger starbursts in galaxies (e.g., Mihos & Hernquist 1996; Taniguchi & Wada 1996), we suggested that the high fraction of [O II] emitters in high-density regions may be driven by interactions and/or mergers. On the other hand, in the previous section, we found that the [O II] fraction in the high-density environment is higher only for high mass ( $M_* \sim 10^{10} - 10^{11} M_\odot$ ) galaxies, while there is no evidence for environmental dependence at  $M_* \lesssim 10^{10} M_\odot$ . Here we study the effects of the interactions and/or mergers on the star formation activity and its environmental dependence as a function of stellar mass.

Following Paper I, we define a galaxy with a close companion as a system with a nearest neighbor within an projected separation of less than 10 arcsec, corresponding to  $< 80$  kpc in proper distance at  $z = 1.2$ . We use galaxies with  $i' < 24$  within a redshift slice of  $\pm \sigma_{\Delta z}$  to search for nearest neighbors, as in the estimate of the local galaxy density (Section 3.1). This redshift slice corresponds to a maximal velocity difference of  $\Delta V \sim 1600$  km  $s^{-1}$ . Using this definition, we identify 222 galaxies with a close companion from the 1446 photo- $z$  selected galaxies. The other galaxies do not have a close companion. We call hereafter these galaxies “non-companion galaxies”.

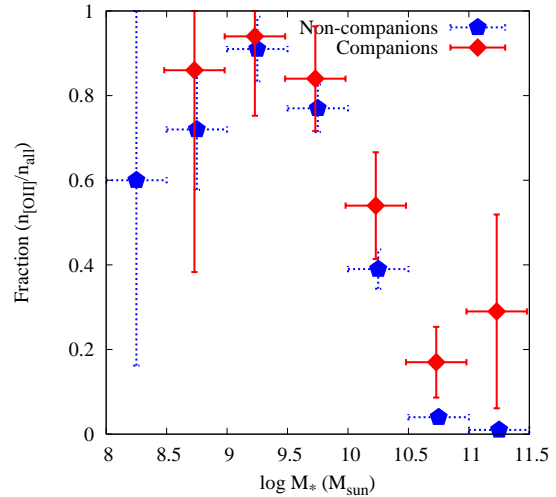


FIG. 5.— The fraction of [O II] emitters as a function of stellar mass for the galaxies with and without a companion. The blue pentagons and red diamonds represent the without companion and with companion samples, respectively. The error bars are the same as Figure 2. Data points for the non-companion and companion samples are plotted with small horizontal offsets for clarity.

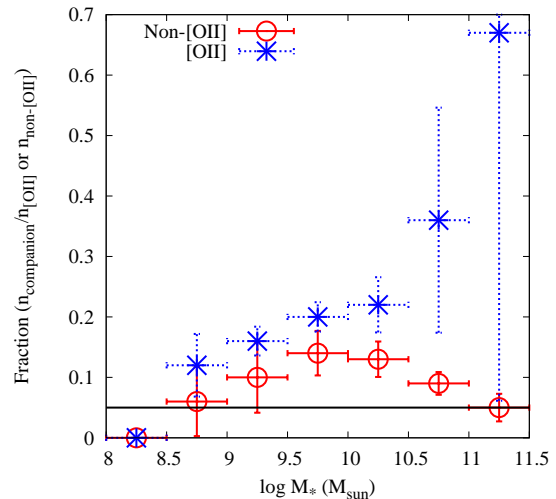


FIG. 6.— The fraction of the galaxies with a companion as a function of stellar mass. The cross and circle points represent [O II] emitters and non-[O II] emitters, respectively. The error bars are the same as Figure 2. The horizontal line shows the probability of the chance alignment calculated from average number density of all photo- $z$  selected galaxies.

The 71% of the galaxies with a close companion are [O II] emitters. The numbers of companion galaxies for each environment and stellar mass are summarized in Table 2. Note that these galaxies may not always be interacting, since the maximum velocity difference of  $\Delta V \sim 1600$  km  $s^{-1}$  is large for interactions or/and mergers. We calculate the probability of chance alignment from the average number density of galaxies and the search area with a radius of 80kpc. The probability of chance alignment is 0.05 in the full sample and 0.02, 0.05, and 0.12 for the low-, intermediate-, high-density environments, respectively. Although the probability of chance alignment is relatively small, we take this effect into account in the following analysis.

TABLE 2  
THE NUMBER OF COMPANIONS IN EACH ENVIRONMENTS AND MASS BINS

log $M_*(M_\odot)$	All samples			[O II] emitters			non-[O II] emitters		
	Low	Intermediate	High	Low	Intermediate	High	Low	Intermediate	High
8 – 8.5	0	0	0	0	0	0	0	0	0
8.5 – 9	2	1	3	1	1	3	1	0	0
9 – 9.5	19	24	4	17	23	4	2	1	0
9.5 – 10	21	56	13	17	47	11	4	9	2
10 – 10.5	8	28	14	6	13	8	2	15	6
10.5 – 11	5	15	3	1	2	2	4	13	1
11 – 11.5	2	4	0	0	2	0	2	2	0
11.5 – 12	0	0	0	0	0	0	0	0	0
Total	57	128	37	42	88	28	15	40	9

In Figure 5, we show the [O II] fraction as a function of stellar mass for the galaxies with and without a companion. While the [O II] fractions for these two samples are similar within the error bars at low mass ( $M_* < 10^{10} M_\odot$ ), the [O II] fraction for the “with companion” sample is  $2.4 \pm 0.5$  times higher than that for the “without companion” sample at  $M_* = 10^{10} - 10^{11.5} M_\odot$ . The difference in [O II] emitter fractions between the two samples appears to increase with increasing stellar mass. Figure 6 shows the relation between the fraction of galaxies with a companion (hereafter “companion fraction”) and stellar mass for [O II] and non-[O II] emitters in all the environments. The horizontal line represents the expected contribution of the chance alignment. The companion fraction for [O II] emitters is higher than that for non-[O II] emitters and the probability of the chance alignment. It is also seen that the companion fraction for [O II] emitters increases with increasing stellar mass, while the fraction for non-[O II] emitters does not. Indeed, it is estimated that the companion fraction for [O II] emitters at high mass ( $M_* = 10^{10} - 10^{11.5} M_\odot$ ) is  $1.5 \pm 0.3$  times higher than that at low mass ( $M_* < 10^{10} M_\odot$ ) and that for non-[O II] emitters at high mass is only  $0.7 \pm 0.2$  times that at low mass. Moreover, at high mass, the companion fraction for [O II] emitters is  $2.8 \pm 0.6$  times higher than that for non-[O II] emitters, while that for [O II] emitters is only  $1.3 \pm 0.3$  times that for non-[O II] emitters at low mass. These results suggest that the star formation activity may be induced by interactions and/or mergers more preferentially in high-mass galaxies.

In order to understand the relation between this result and the environmental dependence of the star formation activity, we also investigate the companion fraction in [O II] emitters as a function of stellar mass in the three different environments (Figure 7). The horizontal lines in the figure represent the probability of the chance alignment for the three environments. It is seen that the companion fraction tends to be higher in the higher-density environment, especially at high stellar mass, although there is the large uncertainty due to the small number statistics. The companion fractions at  $M_* = 10^{10} - 10^{11.5} M_\odot$  in the low-, intermediate-, and high-density environment are estimated to be  $0.2 \pm 0.1$ ,  $0.3 \pm 0.1$ , and  $0.4 \pm 0.1$ , respectively. Although the probability of the chance alignment also tends to be higher in the higher-density environment, the environmental dependence of the companion fraction at high mass ( $M_* = 10^{10} - 10^{11.5} M_\odot$ ) appears to remain even

if we subtract the contribution of chance alignment. We also find that the companion fraction for [O II] emitters in the high- and intermediate environments increases with increasing stellar mass. The plots of Figure 7 are fit with the following relations:  $\text{Fraction}(n_{\text{companion}}/n_{[\text{OII}]}) = (0.03 \pm 0.03) \times \log M_* - (0.16 \pm 0.34)$  for the low-density environment,  $(0.14 \pm 0.02) \times \log M_* - (1.14 \pm 0.21)$  for the intermediate-density environment, and  $(0.08 \pm 0.06) \times \log M_* - (0.47 \pm 0.62)$  for the high-density environment. Although the uncertainty for the high-density environment is relatively large due to the small number statistics, the correlation between the companion fraction and the stellar mass for the intermediate-density environment is evident. Thus the star formation in massive [O II] emitters in higher-density environment may be preferentially triggered by interactions and/or mergers.

Figure 8 shows the average SFR of [O II] emitters with and without a companion as a function of stellar mass. We then apply a linear fit to obtain the relation for the [O II] emitters with and without a companion:  $\log \langle \text{SFR} \rangle = (0.59 \pm 0.11) \times \log M_* - (4.59 \pm 1.01)$  and  $\log \langle \text{SFR} \rangle = (0.52 \pm 0.11) \times \log M_* - (3.98 \pm 1.03)$ , respectively. We find that there is no significant difference between the companion and non-companion samples. Since the [O II] fraction for high-mass galaxies depends on the presence of a close companion as seen above, these results imply that galaxy interaction does not affect SFR in star-forming galaxies but can trigger a larger number of high-mass galaxies to become star forming at all.

#### 4.3. Effects of the Contamination and Incompleteness in the Sample

Here we consider the effects of sample contamination and incompleteness on the results shown in the previous two sections. As mentioned in Section 2.3, the estimated photo- $z$  contamination and incompleteness is  $\sim 20\%$ . Since it is unlikely that the fraction of contamination or incompleteness depends strongly on the local number density of galaxies, it is expected that the contamination and incompleteness could not significantly change the estimation of local galaxy density (although contamination could slightly smear out the density contrast).

The contamination and incompleteness rates are different between the [O II] emitter and non-[O II] emitter samples; the contamination rates for the [O II] emitter sample and for the non-[O II] emitter sample are estimated as 8% and 35%, and the incompleteness rates for

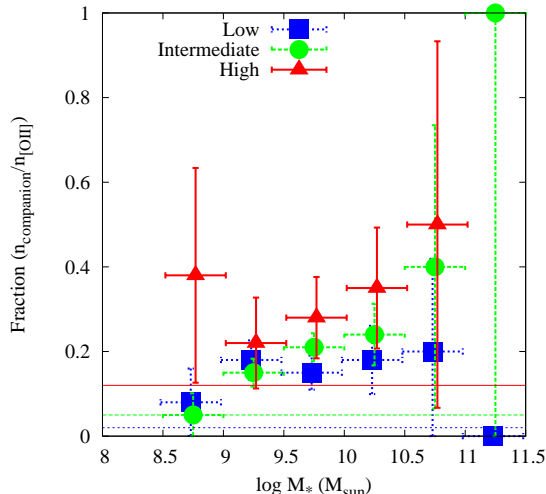


FIG. 7.— The fraction of galaxies with a companion in [O II] emitters as a function of stellar mass in the three different environments. The symbols and error bars are the same as Figure 2. The horizontal blue, green, and red lines show the probabilities of chance alignment calculated from the average number density of galaxies in the low-, intermediate-, and high-density environment, respectively. Data points for the different environments are plotted with small horizontal offsets for clarity.

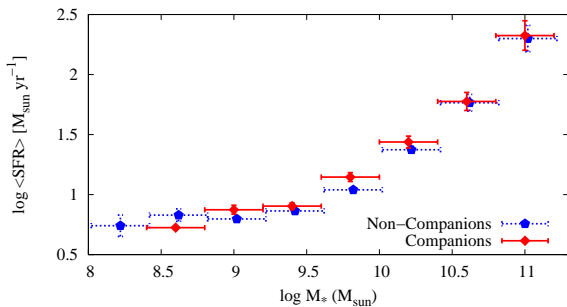


FIG. 8.— The average SFR of [O II] emitters with and without a close companion as a function of stellar mass. The blue pentagons and red diamonds show the non-companions and companions, respectively. The error bars are the same as Figure 4. Data points for the non-companion and companion samples are plotted with small horizontal offsets for clarity.

the [O II] emitter sample and for the non-[O II] emitter sample are 0% and 49%, respectively. Since these difference may affect our results, in the following we discuss their possible effects in detail.

First, we consider possible effects on the [O II] fraction due to contamination and incompleteness. From the contamination and incompleteness rates for the [O II] emitter and non-[O II] emitter samples, we naively expect that the number of [O II] emitters is overestimated by  $\simeq 9\%$ ; i.e.,  $1/(1 - 0.08) \approx 1.09$ . The number of all photo- $z$  selected galaxies (824 [O II] emitters + 622 non-[O II] emitters) is underestimated by  $\simeq 7\%$ ; i.e.,  $(824 + 622)/[824 \times (1 - 0.08) + 622 \times (1 - 0.35)]/0.51 \approx 1.07$ . Thus we may overestimate the overall [O II] fraction by  $\simeq 17\%$ ; i.e.,  $(1 + 0.09)/(1 - 0.07) \approx 1.17$ . In order to investigate effects on the mass and environmental dependence of the [O II] fraction, we check the stellar mass and environment of the contaminant and missed objects with spectroscopic identification. We find that

those galaxies for the [O II] emitter sample and for the non-[O II] emitter sample have stellar mass ranges of  $10^9 M_\odot < M_* < 10^{10} M_\odot$  and  $10^{10} M_\odot < M_* < 10^{11} M_\odot$ , respectively, and exist in various environments (although they are rarer in high-density environments). Thus contamination and incompleteness affect all masses and environments evenly, and so they do not significantly affect the mass and environmental dependence of the [O II] fraction seen in Figure 2. Since the contamination and incompleteness for [O II] emitters are small and do not depend on environment, the stellar mass distribution and the average SFR at a given mass for these galaxies in the different environments (Figures 3 and 4) are also not significantly affected.

Next, we consider effects on the results regarding companions. Since the incompleteness is expected to be independent of the presence or absence of a close companion, the missed objects do not affect the companion fraction. Similarly the contamination from different redshifts is not correlated with the spatial distribution of galaxies at  $z = 1.17 - 1.20$ . Therefore the probability of the contamination from chance alignment is expected to be roughly the probability of the chance alignment calculated in Section 4.2 ( $\simeq 5\%$ ). When the companion fraction is much higher than the probability of the chance alignment, the large contamination could lower the companion fraction. However, high companion fractions are seen for [O II] emitters at high mass in Figure 6. Since the contamination for [O II] emitters is small ( $\simeq 8\%$ ), it does not significantly affect the companion fraction. On the other hand, the contamination rate is  $\simeq 35\%$  for the non-[O II] emitters, but the companion fraction for those galaxies is not much higher than the probability of the chance alignment (Figure 6). Then the effect of the contamination on the companion fraction in the non-[O II] emitter sample also seems to be insignificant, although the companion fraction could be slightly underestimated.

We thus conclude that the contamination and incompleteness of the photo- $z$  sample do not affect significantly our results.

## 5. DISCUSSION

In this paper, we have investigated the relations between the star formation, stellar mass, and environment at  $z \simeq 1.2$  in the COSMOS field. As shown in section 4, our results are different from the observational properties of galaxies in the local universe. Based on our observational results, we discuss possible origins of the difference between  $z \sim 0$  and  $z \sim 1$  from a viewpoint of the evolution of galaxies.

### 5.1. The Observational Properties of Galaxies at $z \simeq 1.2$ in the COSMOS Field

The findings of this study are summarized by the following:

1. At  $M_* \gtrsim 10^{10} M_\odot$ , the fraction of [O II] emitters in high-density environments is  $1.7 \pm 0.4$  times as high as in low- and intermediate-density environments. The fraction of [O II] emitters does not depend on environment at  $M_* \lesssim 10^{10} M_\odot$  (Figure 2).
2. The fraction of [O II] emitters in galaxies with a companion (likely interacting galaxies) is  $2.4 \pm 0.5$



- times higher than that in those without a companion (likely isolated galaxies) over  $M_* \sim 10^{10} - 10^{11.5} M_\odot$  (Figure 5).
3. The fraction of galaxies with a companion for the [O II] emitters at high mass ( $M_* = 10^{10} - 10^{11.5} M_\odot$ ) is  $1.5 \pm 0.3$  times higher than that at low mass ( $M_* < 10^{10} M_\odot$ ), while that for the non-[O II] emitters at high mass is  $0.7 \pm 0.2$  times that at low mass (Figure 6).
  4. The fraction of [O II] emitters with a companion is higher in the higher-density environments (Figure 7). The fractions in the low-, intermediate-, and high-density environment at high mass ( $M_* = 10^{10} - 10^{11.5} M_\odot$ ) are  $0.2 \pm 0.1$ ,  $0.3 \pm 0.1$ , and  $0.4 \pm 0.1$ , respectively.
  5. The average SFR of [O II] emitters strongly correlates with stellar mass in all the environments. For example, the linear fit gives the relation in the high-density environment,  $\log \langle \text{SFR} \rangle = (0.59 \pm 0.08) \times \log M_* - (4.56 \pm 0.78)$ . The SFR at a given mass is independent of the environment and the presence of a close companion (Figures 4 and 8).

From the first item described above, it is expected that high-mass [O II] emitters contribute significantly to the active star formation in high-density regions at  $z \simeq 1.2$ . Moreover, items 2, 3, and 4 suggest that interactions and/or mergers could trigger star formation in massive galaxies preferentially in high-density environments, while the star formation in low-mass galaxies appears to be independent of environment and does not seem to be affected by the interactions and/or mergers. In other words,  $EW([\text{O II}])$  of some inactive high-mass galaxies may become higher due to the active star formation induced by galaxy interactions, and thus we observe such high-mass galaxies as [O II] emitters. On the other hand, considering item 5, it appears that the strength of star formation activity in the star-forming galaxies is not influenced by environmental effects, although the environment and interactions affect the fraction of star-forming galaxies.

The environmental dependence of the [O II] fraction is seen only at high mass. It is interesting to note that the influence of interactions and/or mergers on star formation depends both on environment and stellar mass. This can be interpreted such that massive galaxies need external triggers (i.e., interactions and/or mergers) for active star formation, while the less massive galaxies are form stars regardless of the presence of a close companion. One possible triggering mechanism for less massive galaxies is minor merger events (e.g., Taniguchi & Wada 1996). However, such satellite galaxies would be too faint to be detected in our imaging survey. As an another possible interpretation, it is expected that less massive galaxies contain much gas and can naturally form stars since evolution of those galaxies is slow compared to massive galaxies, which is expected from mass-downsizing (e.g., Cowie et al. 1996).

Therefore, we conclude that the environmental dependence of the [O II] fraction (i.e., the fraction of star-forming galaxies) is seen only at high mass, because 1) interactions and/or mergers induce the star formation

only in massive galaxies and 2) the probability of interactions and/or mergers depends on local galaxy density.

Peng et al. (2010, 2011) recently found that the environment quenching (or the satellite quenching) depends on the local galaxy density but not on the stellar mass of galaxies. We observe a different environmental effect from that found by Peng et al. (2010, 2011), since our results suggest that the influence of interaction and/or mergers depend on both environment and stellar mass.

### 5.2. Implications to the evolution of galaxies from $z \sim 1$ to $z \sim 0$

In the local universe, it is observed that the fraction of red galaxies in high-density environments is higher than that in low-density environments, and this difference becomes larger at lower mass (e.g., Baldry et al. 2006). Namely, the fraction of blue galaxies in high-density environments is lower than that in low-density environments, especially at low mass. Iovino et al (2010) also found a similar trend at  $z < 0.5$ . Furthermore, they found that the fraction of blue galaxies at  $z = 0.6 - 0.8$  does not depend on the environment in  $M_* > 10^{10}$ . These are in contrast to the environmental dependence of the [O II] fraction in massive galaxies at  $z \simeq 1.2$  mentioned above.

Now a question arises: what is the origin of the difference between  $z \sim 1$  and  $z \sim 0$ ? Our results suggest that interactions and mergers are likely to induce star formation in massive galaxies in high-density environments at  $z \simeq 1.2$ , resulting in the observed high [O II] fraction of massive galaxies in high-density environments. These inactive massive galaxies where star formation would be induced by interactions are likely to have some cold gas for star formation. We have also found that the average SFR at a given mass is similar among the different environments and is independent of the presence of a close companion (Figures 4 and 8), the strength of the star formation induced by interactions in massive galaxies does not seem to be significantly different from other massive star-forming galaxies on average. Therefore we expect that there are already some inactive high-mass galaxies with sufficient cold gas for SFR at a given mass at  $z \simeq 1.2$ . On the other hand, the fraction of gas-poor galaxies is higher in higher density regions at low- $z$  (e.g., Giovanelli & Haynes 1985; Bertram et al. 2006). Therefore it is unlikely that a significant starburst occurs in interactions or mergers between gas-poor galaxies (i.e., dry mergers; e.g., Tran et al. 2005; Cattaneo et al. 2008), even though interactions and/or mergers still occur in high-density regions at low- $z$  (e.g., Patton et al. 2011).

In this context, one important difference in galaxies between  $z \sim 1.2$  and low  $z$  is the cold gaseous content. Since galaxies at  $z \sim 1.2$  are in early stages of their evolution, it is likely that their cold gaseous content is, on average, larger than that in galaxies at low  $z$  even if such galaxies are located in relatively high-density regions. It is thus expected that interactions and mergers at  $z \simeq 1.2$  could cause intense star formation more frequently since it is known that interactions and mergers between two gas-rich galaxies (wet mergers) can induce active star formation and rapidly consume the cold gas (e.g., Barton et al. 2000; Woods et al. 2006). In fact, Lin et al. (2008, 2010) suggest that the fraction of dry mergers gradually increases from  $z \sim 1$  to  $z \sim 0$ , while the fraction of wet mergers decreases at the redshift range.

If there are many inactive high-mass galaxies with sufficient cold gas for star formation at  $z \simeq 1.2$  as mentioned above, there may be some mechanisms responsible for quenching star formation in galaxies while retaining their gas. For example, it might be expected that high-mass galaxies have experienced starbursts in the past, and then their gas becomes hot and their star formation stops in spite of the existence of the (hot) gas. Later the hot gas cools down into cold gas, and then high-mass galaxies actively form stars when interactions and/or mergers occur. As another scenario, high-mass galaxies might have consumed most of gas in the past, which is expected from the mass-downsizing of galaxy formation (e.g., Cowie et al. 1996), and the gas density was already too low to cause intense star formation (Kennicutt 1989). However, if interactions can sufficiently perturb the remaining gas, the star formation can be triggered and they can be observed as high-mass star-forming galaxies in high-density environment. In this case, such galaxies immediately consume their gas in the star formation and these massive galaxies in high-density environment are observed to be passive at  $z \lesssim 1$ .

From these considerations, we suggest the following scenario; The high-mass star-forming galaxies for which star formation are induced by interactions and/or mergers contribute significantly to the active star formation in high-density regions at  $z \simeq 1.2$ . These massive star-forming galaxies in high-density regions at  $z \simeq 1.2$  could quickly consume most of the accreted cold gas. If this is the case, the star formation activity may not be enhanced when interactions and/or mergers occurred in high-density environments at lower redshift. In this context, the quenching of star formation in massive galaxies in high density environments is expected to lead to the shift of major star formation in the universe from high-density regions to low-density ones at  $z \lesssim 1$ .

We would like to thank the anonymous referee for her/his very useful comments and suggestions. We also thank all members of the COSMOS team. This work was financially supported in part by the Japan Society for the Promotion of Science (Nos. 17253001, 19340046, 23244031, and 23654068). Y. I. is financially supported by the Japan Society for the Promotion of science (JSPS) through JSPS Research Fellowship for Young Scientists.

## REFERENCES

- Baldry, I. K., et al. 2006, *MNRAS*, 373, 469  
 Balogh, M., et al. 2004, *MNRAS*, 348, 1355  
 Barton, E. J., Geller, M. J., & Kenyon, S. J. 2000, *ApJ*, 530, 660  
 Bertram, T., Eckart, A., Krips, M., Staguhn, J. G., & Jackenberg, W. 2006, *A&A*, 448, 29  
 Bouwens, R. J., et al. 2009, *ApJ*, 705, 936  
 Capak, P. L., Abraham, R. G., Ellis, R. S., Mobasher, B., Scoville, N. Z., Sheth, K., & Koekemoer, A. 2007, *ApJS*, 172, 284  
 Capak, P. L., et al. 2011, in preparation  
 Cardelli, J. A., Clayton, G. C., & Mathis, J. S. 1989, *ApJ*, 345, 245  
 Carter, B. J., Fabricant, D. G., Geller, M. J., Kurtz, M. J., McLearn, B. 2001, *ApJ*, 559, 606  
 Cattaneo, A., Dekel, A., Faber, S. M., & Guiderdoni, B. 2008, *MNRAS*, 389, 567  
 Cooper, M. C., et al. 2008, *MNRAS*, 383, 1058  
 Cowie, L. L., Songaila A., Hu, E. M., & Cohen, J. G. 1996, *AJ*, 112, 839  
 Daddi, E., et al. 2007, *ApJ*, 670, 156  
 Davis, M., et al. 2003, *Proc. SPIE*, 4834, 161  
 Dressler, A. 1980, *ApJ*, 236, 351  
 Dressler, A., et al. 1997, *ApJ*, 490, 477  
 Elbaz, D., et al. 2007, *A&A*, 468, 33  
 Feruglio, C., et al. 2010, *ApJ*, 721, 607  
 Garn, T., et al. 2010, *MNRAS*, 402, 2017  
 Gilbank D. G., et al. 2010, *MNRAS*, 405, 2594  
 Giavalisco, M., et al. 2004, *ApJ*, 600, L93  
 Giovanelli & Haynes 1985, *ApJ*, 292, 404  
 Gomez, P. L., et al. 2003, *ApJ*, 584, 210  
 Goto, T., Yamauchi, C., Fujita, Y., Okamura, S., Sekiguchi, M., Smail, I., Bernardi, M., & Gomez, P. L. 2003, *MNRAS*, 346, 601  
 Gunn, J. E., & Gott, J. R. 1972, *ApJ*, 176, 1  
 Hayashi, M., et al. 2010, *MNRAS*, 402, 1980  
 Hilton, M., et al. 2010, *ApJ*, 718, 133  
 Hogg, D. W., Blanton, M. R., Eisenstein, D. J., et al. 2003, *ApJ*, 585, 5  
 Hopkins, A. M. 2004, *ApJ*, 615, 209  
 Ideue, Y., et al. 2009, *ApJ*, 700, 971  
 Ilbert, O., et al. 2009, *ApJ*, 690, 1236  
 Ilbert, O., et al. 2010, *ApJ*, 709, 644  
 Iovino, A., et al. 2010, *A&A*, 509, 40  
 Janssen, R. A., Franx, M., & Fabricant, D. 2001, *ApJ*, 551, 825  
 Kauffmann, G., White, S. D. M., Heckman, T. M., Menard, B., Brinchmann, J., Charlot, S., Tremonti, C., & Brinkmann, J. 2004, *MNRAS*, 353, 713  
 Kennicutt, R. C. 1983, *ApJ*, 272, 54  
 Kennicutt, R. C. 1989, *ApJ*, 344, 685  
 Kennicutt, R. C. 1998, *ARA&A*, 36, 189  
 Koekemoer, A. M., et al. 2007, *ApJS*, 172, 196  
 Lemaux, B. C., Lubin, L. M., Sharpley A., Kocevski, D., Gal, R. R., & Squires, G. K. 2010, *ApJ*, 716, 970  
 Lewis, I., et al. 2002, *MNRAS*, 334, 673  
 Lilly, S., et al. 2007, *ApJS*, 172, 70  
 Lilly, S., et al. 2011, in preparation  
 Li, I. H., et al. 2011, *MNRAS*, 411, 1869  
 Lin, L., et al. 2008, *ApJ*, 681, 232  
 Lin, L., et al. 2010, *ApJ*, 718, 1158  
 Madau, P., Ferguson, H. C., Dickinson, M. E., Giavalisco, M., Steidel, C. C., & Fruchter, A. 1996, *MNRAS*, 283, 1388  
 Mahajan, S., Haines, C. P., & Raychaudhury, S. 2010, *MNRAS*, 404, 1745  
 Mateus, A., & Sodr e, L. 2004, *MNRAS*, 349, 1251  
 Mihos, J. C., & Hernquist, L. 1996, *ApJ*, 464, 641  
 Patton, D. R., Ellison, S. L., Simard, L., McConnachie, A. W., & Mendel, T. J. 2011, *MNRAS*, 412, 591  
 Peng, Y.-J., et al. 2010, *ApJ*, 721, 193  
 Peng, Y.-J., Lilly, S. J., Renzini, A., & Marcella, C. 2011, *ApJ*, submitted [arXiv:1106.2546]  
 Scoville, N. Z., et al. 2007a, *ApJS*, 172, 1  
 Scoville, N. Z., et al. 2007b, *ApJS*, 172, 150  
 Shioya, Y., et al. 2008, *ApJS*, 175, 128  
 Sobral, D., Best, P. N., Smail, I., Geach, J. E., Cirasuolo, M., Garn, T., & Dalton, G. B. 2011, *MNRAS*, 411, 675  
 Stern, D., et al. 2005, *ApJ*, 631, 163  
 Takahashi, M. I., et al. 2007, *ApJS*, 172, 456  
 Taniguchi, Y., et al. 2007, *ApJS*, 172, 9  
 Taniguchi, Y., & Wada, K. 1996, *ApJ*, 469, 58  
 Thomas, D., Maraston, C., Schiawinski, K., Sarzi, M., & Silk, J. 2010, *MNRAS*, 404, 1775  
 Tran, K.-V. H., et al. 2005, *ApJ*, 627, L25  
 Woods, D. F., Geller, M. J., & Barton, E. J. 2006, *AJ*, 132, 197  
 Yan, R., Newman J. A., Faber S. M., Konidaris., Koo D., & Davis M. 2006, *ApJ*, 648, 281